

Impact of \mathcal{T} -symmetry on decoherence and control for an electron spin in a synthetic spin-orbit field

Peihao Huang^{1*} and Xuedong Hu²

¹*Shenzhen Institute for Quantum Science and Engineering,*

Southern University of Science and Technology, Shenzhen 518055, China

²*Department of Physics, University at Buffalo, SUNY, Buffalo, New York 14260*

(Dated: December 22, 2024)

Abstract

The electric control of a spin qubit in a quantum dot relies on spin-orbit coupling (SOC). Here, we show that the time-reversal symmetry (\mathcal{T} -symmetry) of the intrinsic SOC leads to not only the traditional van Vleck cancellation known for spin relaxation, but also vanishing spin dephasing to the lowest order of SOC, which we term as “longitudinal spin-orbit field cancellation”. On the other hand, a micro-magnet used in recent experiments creates a synthetic SOC that breaks \mathcal{T} -symmetry, which helps eliminate both the “van Vleck cancellation” and the “longitudinal spin-orbit field cancellation”. This modification removes the dependence on the quantization magnetic field of the effective magnetic field $\vec{\Omega}$ experienced by the spin qubit, and in principle allows a longitudinal component for $\vec{\Omega}$. Consequently, spin relaxation and dephasing are qualitatively modified compared with the case of the intrinsic SOC. We further demonstrate that the longitudinal component of $\vec{\Omega}$ could enable novel schemes for spin coupling and manipulation, with potential applications in semiconductor quantum computing.

* huangph@sustech.edu.cn

I. INTRODUCTION

An electron spin qubit in a semiconductor quantum dot (QD) is a promising candidate for quantum information processing due to the long spin coherence time and possible scalability [1–6]. Exciting progress has been made in recent years on spin qubits in QDs. High fidelity spin manipulation has been realized in a Si QD [7, 8]; Strong coupling has been achieved between a spin qubit in a Si/SiGe QD and a superconducting resonator [9–11]; Two-qubit CPHASE and CNOT gates have been realized based on the exchange interaction [12–14]; And up to nine controllable QDs have been demonstrated [15, 16].

A driving force behind many of the experimental achievements is the introduction of a micromagnet next to the QDs. Such a micromagnet creates an inhomogeneous magnetic field, which acts as a synthetic spin-orbit coupling (s-SOC) and allows fast electric dipole spin resonance (EDSR) of a spin qubit driven by an electric field [7, 17–21] and strong spin-photon coupling [9, 10, 22, 23]. However, while such an electric field could be applied or from a resonator [7, 9, 10, 17–22], it could also be from electrical noises [7, 24–26]. In other words, the s-SOC opens additional spin decoherence channels. Various aspects of s-SOC-enabled decoherence have been explored previously, such as spin relaxation [17, 24, 25] and dephasing [7, 26, 27], and effects of the magnetic noise from the micro-magnets [28, 29]. However, there is still a lack of understanding on how the types of SOC differ in principle, and how such difference affects spin properties in QD systems.

In this work, we show that the most important qualitative difference between s-SOC and the intrinsic SOC (i-SOC) is with respect to the time-reversal symmetry (\mathcal{T} -symmetry): s-SOC breaks it, while i-SOC preserves it. For the case of the i-SOC, we show that it results in not only the traditional van Vleck cancellation [30, 31], but also vanishing longitudinal component of the effective magnetic field, which we term as “longitudinal spin-orbit field cancellation”. For the case of the s-SOC, consequences of the broken \mathcal{T} -symmetry is the disappearance of the Van Vleck cancellation and the “longitudinal spin-orbit field cancellation”. Therefore, spin relaxation has a different magnetic field dependence in the presence of s-SOC as compared to i-SOC, and longitudinal effective magnetic field is allowed at the lowest order perturbation, so that electrical noise could cause pure dephasing of a spin qubit at the lowest order, contrary to the case of i-SOC. Furthermore, we show that s-SOC could provide new ways for spin-spin coupling and spin manipulation. Specifically, the longitudi-

nal effective magnetic field could enable a form-variable spin-spin coupling through a cavity, and the strong driving of a dressed spin qubit in a QD system. Finally, the connection between spin qubit properties and \mathcal{T} -symmetry of the SOC is general, which can be applied to many other physical systems.

II. RESULTS

In this section, we introduce the model Hamiltonian, summarize the derivation of an effective Hamiltonian, and clarify the role of \mathcal{T} -symmetry. We then systematically examine the consequences of the broken \mathcal{T} -symmetry of SOC in terms of spin relaxation, spin pure dephasing, spin-photon coupling, and the strong driving of a spin qubit.

We consider a single electron in a gate-defined QD [see Figure 1 (a)]. The QD confinement in the [001]-direction (defined as z-axis) is provided by the interface electric field, while the in-plane (i.e. xy plane) confinement is provided by top gates. A micromagnet (e.g. a cobalt magnet) is deposited over the QD and polarized by an applied magnetic field. We separate the total magnetic field into two parts $\vec{B} = \vec{B}_0 + \vec{B}_1$, where \vec{B}_0 (\vec{B}_1) is the position-independent (position-dependent inhomogeneous) magnetic field. The Hamiltonian for this model system is thus

$$H = H_Z + H_d + H_{SO} + V_{ext}(\vec{r}). \quad (1)$$

Here $H_Z = \frac{1}{2}g\mu_B\vec{\sigma} \cdot \vec{B}_0$ is the Zeeman Hamiltonian due to the position independent field, where g is the effective g-factor, and $\vec{\sigma}$ is the Pauli operator for the electron spin. $H_d = \frac{p^2}{2m^*} + \frac{1}{2}m^*\omega_d^2 r^2$ is the usual electron 2D orbital Hamiltonian in a single QD, where $\vec{r} = (x, y)$ and $\vec{p} = -i\hbar\nabla + (e/c)\vec{A}(\vec{r})$ are the in-plane 2D coordinate and kinetic momentum operators ($e > 0$), and ω_d is the characteristic frequency of the in-plane confinement. The vertical dynamics is neglected due to the strong confinement at the interface. $V_{ext}(\vec{r})$ is the electric potential due to electrical noise or manipulation field. Lastly, the s-SOC term H_{SO} is due to the Zeeman effect in the position-dependent inhomogeneous magnetic field \vec{B}_1 . Keeping the lowest order position dependence,

$$H_{SO} = \frac{1}{2}g\mu_B\vec{\sigma} \cdot \vec{b}_1 x, \quad (2)$$

where the inhomogeneity is assumed in the x -direction without loss of generality, and the gradient of the inhomogeneous magnetic field, $\vec{b}_1 \equiv \partial\vec{B}_1/\partial x \Big|_{x=0} \equiv [b_{1l}, 0, b_{1t}]$, is the coupling

constant of the s-SOC.

Critical role of \mathcal{T} -symmetry— Assuming that the energy scale of SOC is much less than the orbital and Zeeman energy, we perform a Schrieffer-Wolff (SW) transformation $H_{eff} = e^S H e^{-S}$ to eliminate H_{SO} in the leading order by requiring that $[H_d + H_Z, S] = H_{SO}$ [32, 33]. The transformation generator S can be formally written as

$$S = \sum_{m=0}^{\infty} (L_Z L_d^{-1})^m L_d^{-1} H_{SO}, \quad (3)$$

where the super-operators L_d and L_Z are defined such that $L_d \mathcal{O} = [H_d, \mathcal{O}]$ and $L_Z \mathcal{O} = [H_Z, \mathcal{O}]$ for any given operator \mathcal{O} . Once S is given, an effective spin Hamiltonian $H_{eff} = H_Z + [S, V_{ext}]$ can be obtained.

The \mathcal{T} -symmetry of H_{SO} plays a critical role in the SW transformation. For any SOC, the generator S can be formally rewritten as $S = \vec{f} \cdot \vec{\sigma}$, where \vec{f} contains the orbital operators. Since both the ground orbital state $|\psi\rangle$ and $V_{ext}(\vec{r})$ are time-reversal symmetric (TRS), the matrix element $\langle \psi | [\vec{f}, V_{ext}(\vec{r})] | \psi \rangle$ would be finite only when \vec{f} is also TRS. Given that spin operator $\vec{\sigma}$ is time-reversal asymmetric (TRA), only the TRA terms in S could contribute to the effective spin Hamiltonian H_{eff} .

For the TRA s-SOC, the first term $L_d^{-1} H_{SO}$ in S is TRA and is allowed. For the TRS i-SOC, on the other hand, the first term in S is TRS so that it is forbidden. The lowest order contribution is from the next order term $L_Z L_d^{-2} H_{i-SOC}$, which is TRA and is allowed, with L_Z involving Zeeman term H_Z that breaks \mathcal{T} -symmetry (see Methods). Clearly, the different \mathcal{T} -symmetries of the s-SOC and the i-SOC ensures that their contribution to the spin Hamiltonian are of different orders in E_Z/E_d , and leads to qualitatively different results.

More specifically, for i-SOC, the lowest-order contribution is from the second term in S , which is linearly proportional to B_0 . One consequence is an extra B_0^2 dependence of spin relaxation (shown below), consistent with the so-called van Vleck cancellation [30, 31]. Moreover, given that all the higher-order terms in S contains the L_Z operator, and the property $L_Z(\vec{\varepsilon} \cdot \vec{\sigma}) \propto (\vec{B}_0 \times \vec{\varepsilon}) \cdot \vec{\sigma}$ is satisfied by any vector $\vec{\varepsilon}$, the resulting effective spin-electric coupling $[S, V_{ext}] \propto (\vec{B}_0 \times [\vec{\varepsilon}, V_{ext}]) \cdot \vec{\sigma}$ contains only transverse coupling. In other words, the effective field sensed by the spin is always transverse. Therefore, the conservation of the \mathcal{T} -symmetry of the i-SOC results in the vanishing longitudinal effective magnetic field to any order in the perturbative expansion of Eq. (3). We term this effect “longitudinal spin-orbit field cancellation”, in analogy to the van Vleck cancellation for spin relaxation.

In comparison, the breaking of \mathcal{T} -symmetry by the s-SOC means that generator S could contain a term that is independent of L_Z operator, therefore removing the condition for both the van Vleck cancellation and the “longitudinal spin-orbit field cancellation”. Thus, for s-SOC, the effective magnetic field could be independent of B_0 , and the longitudinal effective magnetic field is allowed.

Our argument here does not assume any specific form of the SOC and H_d . It is thus generally applicable to many different physical systems as long as SOC is smaller in magnitude than the orbital and Zeeman splitting. For example, the results can be used for an electron spin qubit in a double quantum dot with or without a micro-magnet, or an electron spin at donor(s) with a Coulombic confinement. It should also be applicable to other forms of SOC.

Effective Hamiltonian— With the energy scale of s-SOC satisfying $\|H_{s-SOC}\| \ll E_Z = g\mu_B B_0 \ll E_d = \hbar\omega_d$, to the lowest order of H_{s-SOC} and E_Z/E_d , we have $S \approx L_d^{-1} H_{SOC}$. Using this generator, the effective spin Hamiltonian is (see Methods)

$$H_{eff} = \frac{1}{2} g\mu_B \vec{\sigma} \cdot (\vec{B}_0 + \vec{\Omega}), \quad (4)$$

where $\vec{\Omega} = -\vec{b}_1 \partial_x V_{ext}/(m^* \omega_d^2)$ is the effective magnetic field generated from the electric potential through the QD displacement $\delta_x = -\partial_x V_{ext}/(m^* \omega_d^2)$ and the s-SOC.

As we discussed in the previous section, the effective field $\vec{\Omega}$ generated by $S = L_d^{-1} H_{SOC}$ has some distinctive properties as a result of the elimination of both the van Vleck cancellation and the longitudinal spin-orbit field cancellation. First, it can have a longitudinal component parallel to the constant applied magnetic field \vec{B}_0 . If V_{ext} is a potential from electrical noise, the corresponding effective magnetic noise $\vec{\Omega}$ would lead to both spin relaxation and pure dephasing (see Figure 1 (b)). Second, $\vec{\Omega}$ is independent of B_0 . Both are different from the case of the i-SOC, where the effective noise magnitude is linearly proportional to B_0 , and induces only spin relaxation [32, 33]. Below we explore consequences of these new characteristics of the effective field $\vec{\Omega}$.

Spin Relaxation—Spin relaxation time gives the upper limit of spin coherence time, when pure dephasing vanishes. Suppose the direction of magnetic field \vec{B}_0 (assumed along the x -axis in this work) is defined as the new Z -axis, while X - and Y -axis are orthogonal to the Z -axis (see Figure 1 (b)), the relaxation rate is then given by $1/T_1 = S_{XX}(\omega_Z) + S_{YY}(\omega_Z)$ [32, 33], where $S_{ii}(\omega)$ is the power spectral density of the magnetic noise in the i th direction, and $\omega_Z = g\mu_B B_0/\hbar$ is the Larmor frequency. In our single QD system, spin relaxation is

determined by the transverse magnetic noise $\Omega_X = -b_{1t}\partial_x V_{ext}/(m^*\omega_d^2)$, and the relaxation rate is

$$1/T_1 = \left[\frac{g\mu_B b_{1t}}{2\hbar m^* \omega_d^2} \right]^2 S_{FF}(\omega_Z), \quad (5)$$

where $S_{FF}(\omega)$ is the spectral density of the force correlation of the noise [34].

Qualitatively, spin relaxation depends on the transverse field gradient, with $1/T_1 \propto b_{1t}^2 = (\partial B_z / \partial x)^2$. It also has a strong dependence on the QD confinement, $1/T_1 \propto 1/\omega_d^4$, and is suppressed in a smaller QD. Lastly, the dependence of spin relaxation on the magnetic field B_0 is given by $S_{FF}(\omega_Z)$ (neglecting the weak dependence of b_{1t} on B_0 when the micromagnet is saturated), as we discuss in more detail below.

Figure 2(a) shows the spin relaxation rate as a function of the magnetic field B_0 due to deformation coupling to phonons or dipole coupling to Johnson noise in silicon (parameters are listed in Methods). Here we neglect the valley states (from conduction band degeneracy) in silicon by assuming that the intra-valley spin-orbit mixing dominates. Spin relaxation due to phonon emission mediated by s-SOC shows a B_0^5 dependence, $1/T_1 \propto B_0^5$, in contrast to the B_0^7 dependence in the case of the i-SOC [32, 35]. The extra B_0^2 dependence is due to the \mathcal{T} -symmetry of the i-SOC that leads to the Van Vleck cancellation. For the same reason, spin relaxation due to Johnson noise mediated by s-SOC shows a linear B_0 dependence, $1/T_1 \propto B_0$, in contrast to the B_0^3 dependence in the case of the i-SOC [33]. Consequently, at low B -field spin relaxation is dominated by Johnson noise, while at higher B -field it is dominated by phonon emission, as shown in Figure 2. The calculated spin relaxation rate grows from 0.01 s^{-1} to 1000 s^{-1} as B_0 increases from 0.2 T to 10 T .

The spin relaxation channel discussed here can be relevant in a silicon QD experiment when the magnetic field is relatively high. For comparison, let us consider the case of an electron spin in a silicon QD without a micromagnet. Here spin relaxation is mostly due to phonon and Johnson noise via the i-SOC induced spin-valley or spin-orbit mixing [34]: At low magnetic field, spin relaxation is dominated by the spin-valley mixing, where $1/T_1 \sim 1$ to 1000 s^{-1} . While at high magnetic field (when Zeeman splitting is bigger than valley splitting, i.e. $B_0 > 3 \text{ T}$ if the valley splitting is 0.3 meV), spin relaxation via spin-valley mixing is strongly suppressed, and spin relaxation is dominated by spin-orbit mixing [corresponding to the case of i-SOC+ph in Figure 2 (a)]. The numerical estimate in Figure 2(a) thus indicates that the relaxation due to phonon noise via a synthetic SOC can be dominant in a silicon QD at relatively high magnetic field. Recent experiments in

a silicon QD with micromagnets show that spin relaxation at high magnetic field has B_0^5 dependence [24, 25], deviating from the B_0^7 dependence normally observed in silicon without micromagnets [36–38], but consistent with our theoretical results here.

Pure dephasing—The breaking of \mathcal{T} -symmetry of s-SOC allows a longitudinal effective magnetic field, so that electrical noise can cause pure dephasing of the electron spin at the lowest order of s-SOC, which i-SOC does not allow [32, 33]. Such charge noise induced dephasing has indeed been measured and discussed in Refs. [7, 26], where it has been asserted that the $1/f$ charge noise induced spin pure dephasing is the dominant dephasing channel in the presence of s-SOC. Below we examine the qualitative dependence of the spin pure dephasing on system parameters such as the QD size and the field gradient, and give some numerical results.

Pure dephasing is determined by the spectral density $S_{ZZ}(\omega)$ of the longitudinal noise [39, 40]. Suppose the spectral density of the potential fluctuation of $1/f$ charge noise is $S_{1/f} = A/\omega$, where A is the noise amplitude. For the spin qubit, we then have $S_{ZZ}(\omega) = A_{eff}/\omega$, where $\sqrt{A_{eff}} = \sqrt{A} [g\mu_B b_{1l}/(2\hbar m^* \omega_d^2 l_0)]$ is the amplitude of the effective magnetic noise, and the length l_0 converts the electric potential to the field strength of the charge noise.

The magnetic noise amplitude $\sqrt{A_{eff}}$ depends on the longitudinal field gradient and the orbital splitting as $\sqrt{A_{eff}} \propto b_{1l}/\omega_d^2$, consistent with the intuitive argument given in the supplementary material in Ref. [7]. We emphasize here that this intuition works only in the case for the s-SOC, where the \mathcal{T} -symmetry is broken, but does not work in the case for the i-SOC [33]. Due to the initial Gaussian time dependence for the off-diagonal density matrix element, the spin pure dephasing rate $1/T_\varphi \propto \sqrt{A_{eff}}$ [40]. Thus the pure dephasing rate is determined by the amplitude of the $1/f$ charge noise and system parameters as

$$1/T_\varphi \propto \frac{b_{1l}\sqrt{A}}{\omega_d^2}. \quad (6)$$

Figure 2(b) shows the spin dephasing rate with or without echo as a function of b_{1l} due to $1/f$ charge noise. The dephasing rate is extracted numerically from the dynamics as shown in the inset (calculated similarly as in Ref. [40]). The spin dephasing rate $1/T_\varphi$ (or $1/T_{\varphi,echo}$) has an approximately linear dependence on the magnetic field gradient b_{1l} , consistent with the expectation based on the analytical expressions. Quantitatively, the dephasing rate goes from 1600 s^{-1} to 18000 s^{-1} (or from 460 s^{-1} to 6000 s^{-1} with spin echo) as the magnetic

field gradient b_{1l} increases from 0.1 mT/nm to 1 mT/nm.

The pure dephasing rate due to charge noise can be compared with other possible dephasing mechanisms. For an electron spin in a QD without a micromagnet, nuclear spin noise is a major source for spin dephasing, with spin dephasing time measured to be 360 ns ($1/T_2^* \sim 2.7 \times 10^6$ s $^{-1}$) in natural silicon, and as long as 120 μ s ($1/T_2^* \sim 8 \times 10^3$ s $^{-1}$) in isotopically enriched ^{28}Si [12]. Thus, our numerical estimate indicates that dephasing due to charge noise via an s-SOC can be dominant when b_{1l} is bigger than 0.5 mT/nm (also dependent on the charge noise amplitude) in an isotopically enriched silicon QD. The dominance of charge-noise-induced pure dephasing has been observed in recent experiments [7, 26].

To suppress pure dephasing from charge noise and improve spin coherence in the presence of s-SOC, a straightforward approach is to reduce longitudinal field gradient b_{1l} . However, Maxwell equations for the magnetic field dictate that gradient of the magnetic field along different directions are related and have to be accounted for. For example, according to the Maxwell equations $\nabla \cdot \vec{B} = 0$ and $\nabla \times \vec{B} = 0$, in addition to $b_{1l} = \partial B_x / \partial x$ and $b_{1t} = \partial B_z / \partial x$, the gradient $\partial B_z / \partial z$ and $\partial B_x / \partial z$ would have to be finite as well (all other gradients can be zero if considering the translational symmetry along y). We emphasize that, to optimize the operation of the spin qubit system, we need to consider field gradient and confinement together. We neglected the effects of the gradient $\partial B_z / \partial z$ and $\partial B_x / \partial z$ in our case because they are along the strong confinement direction z , thus, only the gradient b_{1l} and b_{1t} are necessary to be taken into account. In this case, we propose to adjust the quantization field \vec{B}_0 , such that \vec{B}_0 is perpendicular to the vector $\partial \vec{B} / \partial x = (b_{1l}, 0, b_{1t})$, then, the induced effective magnetic field becomes perpendicular to the quantization axis, consequently, the pure dephasing from charge noise can be minimized, while the transverse magnetic field is maximized for enhanced EDSR.

S-SOC enabled spin-photon coupling—Spin qubit communication and coupling via a cavity could be a key ingredient to a scalable quantum computer, and have generated extensive theoretical and experimental explorations [9, 10, 22, 41–43]. With magnetic coupling too weak to be useful, spin-photon coupling via the cavity electric field, assisted by i-SOC or s-SOC, has become the only realistic way to reach the strong-coupling limit, and has recently been demonstrated experimentally [9, 10]. As we have shown above, the breaking of \mathcal{T} -symmetry by the s-SOC results in qualitative differences for spin-electric-field coupling compared with the case of i-SOC, which could lead to modifications to the behavior

of spin-cavity and spin-spin interaction via a cavity. Below, we examine the properties of spin-photon coupling between a spin qubit and a superconducting resonator.

To enhance the cavity electric field, we assume that two gates of the QD are connected to the electrodes of a superconducting resonator [9, 10, 43], so that the electric field $E = -\partial_x V_{ext}/|e|$ in the effective spin Hamiltonian is given by the electric field E_{sc} across the QD due to the voltage difference of the center pin and ground of the resonator. The voltage operator in the resonator is given by $V_{sc} = V_{zpf}(a^\dagger + a)$, where a is the photon annihilation operator in the single-mode superconducting resonator. The voltage $V_{zpf} = \omega_0 \sqrt{\hbar Z_0}$ is the voltage amplitude due to the zero-point fluctuation (ZPF) in the resonator, where ω_0 is the resonator frequency and Z_0 is the characteristic impedance of the resonator. Therefore, the electric field operator becomes $E_{sc} = E_{zpf}(a^\dagger + a)$, where $E_{zpf} = V_{zpf}/d_0$ and d_0 (about the QD size) is the length for the voltage drop. The spin-photon coupling Hamiltonian thus takes the form

$$H_{s-ph} = g_{s,t}(\sigma_+ a + a^\dagger \sigma_-) + g_{s,l} \sigma_Z (a + a^\dagger), \quad (7)$$

where $\sigma_\pm \equiv \sigma_X \pm i\sigma_Y$ is the spin creation or annihilation operator. The strength for the transverse and the longitudinal spin-photon coupling are given by $g_{s,t} = -\frac{eg\mu_B b_{1t}}{2m^* \omega_d^2} \omega_0 \sqrt{\hbar Z_0}/d_0$, and $g_{s,l} = -\frac{eg\mu_B b_{1l}}{2m^* \omega_d^2} \omega_0 \sqrt{\hbar Z_0}/d_0$. In comparison, for i-SOC and at low magnetic field ($g\mu_B B_0 \ll \hbar\omega_d$), $g_{s,t, isoc} = 0$, and $g_{s,t, isoc} = -\frac{eg\mu_B B_0}{\lambda_{so} m^* \omega_d^2 d_0} \omega_0 \sqrt{\hbar Z_0}$, where $\lambda_{so} = \hbar/(m^* \alpha)$ is the effective length of i-SOC, with α being the Rashba SOC constant [33].

The spin-photon coupling strength $g_{s,t}$ and $g_{s,l}$ have linearly dependence on the resonator frequency ω_0 , and $\sqrt{Z_0}$ dependence with the resonator characteristic impedance. The coupling strength $g_{s,t}$ and $g_{s,l}$ have no dependence with the magnetic field B_0 . The coupling strengths have strong dependence with the size of the QD, with $g_{s,t}, g_{s,l} \propto 1/(\omega_d^2 d_0) \propto r_{QD}^3$, where r_{QD} is the size of the QD. The spin-photon coupling strength $g_{s,t}$ ($g_{s,l}$) has linear dependence on the transverse (longitudinal) field gradient, with $g_{s,t} \propto b_{1t}$ ($g_{s,l} \propto b_{1l}$).

Figure 3 shows the spin-photon transverse coupling strengths as functions of the magnetic field B_0 . The coupling strength $g_{s,t}$ shows no B_0 dependence, in contrast to the linear B_0 dependence for $g_{s,t, isoc}$. The extra B_0 dependence is due to the \mathcal{T} -symmetry of the i-SOC that leads to the Van Vleck cancellation. Indeed, the ratio of the two transverse spin-photon coupling strength satisfies

$$\frac{g_{s,t}}{g_{s,t, isoc}} = \frac{b_{1t} \lambda_{so}}{B_0}, \quad (8)$$

which is independent of the quantum dot and cavity parameters such as ω_d and Z_0 . With b_{1t} fixed by the fabrication and λ_{so} fixed by the material and the interface electric field, B_0 becomes an important indicator of the coupling strengths. Specifically, $g_{s,t}$ can be much stronger than $g_{s,t,iso}$ at lower magnetic fields. For example, $g_{s,t}$ is about $5 \times 10^5 \text{ s}^{-1}$, and does not change as B_0 increases, while $g_{s,t,iso}$ grows from $5 \times 10^3 \text{ s}^{-1}$ to 10^5 s^{-1} as B_0 increases from 0.1 T to 3 T. The result suggests that spin-photon strong coupling is possible even at low magnetic field, which is an important consideration when integrating a spin system with a superconducting resonator. Moreover, $g_{s,t}$ does have a strong dependence on the QD confinement in the form of $1/\omega_d^2$. Thus when the QD is bigger, for example when $\hbar\omega_d = 1 \text{ meV}$, the coupling strength increases to 10^7 s^{-1} (about 50 times faster than the case when $\hbar\omega_d = 8 \text{ meV}$). However, for a larger dot d_0 may have to be larger as well, making the increase less dramatic. In short, benchmarked against spin dephasing rate, the strong coupling limit can be achieved more easily for the s-SOC than the case of the i-SOC at lower magnetic field.

Beside the transverse coupling, s-SOC also allows longitudinal coupling between a spin qubit and a superconductor resonator. The longitudinal coupling $g_{s,l}$ is in general finite in contrast to the vanishing $g_{s,l,iso}$ in the case of the i-SOC. The magnitude of $g_{s,l}/g_{s,t}$ depends on the ratio of longitudinal and transverse gradient of magnetic field, with $g_{s,l}/g_{s,t} = b_{1l}/b_{1t}$. Its presence would modify the effective spin coupling mediated by a resonator, as we discuss below, and could be used for measurement and manipulation of a dressed qubit.

Spin-spin coupling of a variable form mediated by s-SOC and a cavity—
When spin-photon strong coupling limit is achieved, effective two-qubit coupling can be realized between remote spin qubits. Consider two spin qubits coupled simultaneously to a resonator. The total Hamiltonian is given by $H_{2Q} = E_0 a^\dagger a + \sum_i \frac{\omega_{Z,i}}{2} \sigma_{Z,i} + \sum_i [g_{s,t,i}(\sigma_{+,i}a + a^\dagger\sigma_{-,i}) + g_{s,l,i}\sigma_{Z,i}(a + a^\dagger)]$, where $\omega_{Z,i}$ is the frequency of each qubit, $g_{s,t,i}$ and $g_{s,l,i}$ are the transverse and the longitudinal coupling strength of each spin qubit to the resonator. Using a Schrieffer-Wolff transformation, an effective two-qubit interaction Hamiltonian can be obtained as

$$\tilde{H}_{int} = J_{XX}(\sigma_{+,1}\sigma_{-,2} + \sigma_{+,2}\sigma_{-,1}) + J_{ZZ}\sigma_{Z,1}\sigma_{Z,2}/2, \quad (9)$$

where $J_{XX} = \frac{g_{s,t}^2}{E_Z - E_0}$ and $J_{ZZ} = -\frac{4|g_{s,l}|^2}{E_0}$ are the effective transverse and longitudinal two-qubit coupling strength. Compare with the normal $\sigma_X\sigma_X$ coupling via the transverse spin-

photon coupling [44–46], an effective $\sigma_Z\sigma_Z$ coupling also arises due to the presence of the longitudinal spin-photon coupling, which provides an extra tool for the design of the coupling between qubits. For example, one can now tune the system Hamiltonian to simulate the Heisenberg model, XXZ model, etc. In contrast, with i-SOC, the effective coupling is fixed to be an XX Hamiltonian.

“Ultra-strong” longitudinal EDSR— In a conventional spin resonance experiment, a constant magnetic field establishes the quantization axis of the spins, while a small transverse AC magnetic field is used to flip the spins. The same principle is behind EDSR experiments (and our considerations so far in this manuscript) in the context of s-SOC [7, 17, 47–51]. Here we show that the longitudinal effective magnetic field induced by the s-SOC opens a new avenue for spin manipulation, allowing possibly “ultra-strong” longitudinal EDSR driving of a single-electron spin qubit, where multi-photon resonance is possible [52, 53].

We consider here a two-tone oscillating electric field $\vec{E}(t)$ that is applied along the x -axis, $\vec{E}(t) = \sum_{k=1,2} \vec{E}_{k,max} \cos(\omega_k t + \phi_k)$, where $k = 1, 2$ are for a microwave and a radio frequency (rf) components, $\vec{E}_{k,max}$ is the field magnitude, and ω_k and ϕ_k are the frequency and the phase of the field. Driven by this electric field, the electron spin experiences an effective oscillating magnetic field via the s-SOC. The driven spin Hamiltonian can be expressed as

$$H_0 = \frac{\omega_Z}{2} \sigma_Z + \sum_k (\Omega_{k,t} \sigma_X + \Omega_{k,l} \sigma_Z) \cos(\omega_k t + \phi_k), \quad (10)$$

where $\Omega_{k,t} = -g\mu_B b_{1t} \frac{eE_{k,max}}{2m^* \omega_d^2}$ and $\Omega_{k,l} = -g\mu_B b_{1l} \frac{eE_{k,max}}{2m^* \omega_d^2}$ are the maximum transverse and longitudinal magnetic field the spin experiences. While the transverse component $\Omega_{1,t}$ is normally used for spin manipulation, below we show that the longitudinal component $\Omega_{k,l}$ provides another channel for spin manipulation.

When the microwave frequency is nearly resonant with the spin Larmor frequency, the dressed spin qubit in the rotating frame (RF) that rotates at ω_1 is governed by

$$H_{\text{driven}} \approx \frac{\Delta}{2} \sigma_Z + \Omega_{1,t} \sigma_X + \Omega_{2,l} \sigma_Z \cos(\omega_2 t + \phi_2), \quad (11)$$

where $\Delta = \omega_Z - \omega_1$ is the microwave detuning from the Zeeman frequency, and the dressed spin qubit is defined by the eigenstates of $H_{0,\text{driven}} = \frac{\Delta}{2} \sigma_Z + \Omega_{1,t} \sigma_X$ in the RF. Notice that the $\Omega_{1,l}$ term has been omitted since its effect is negligible when $\omega_1 \gg \Omega_{1,t}, \Delta$. The $\Omega_{2,t}$ term has also been omitted since $\omega_1 \pm \omega_2$ is always far off-resonance from the frequency of the dressed spin-qubit in the RF. Clearly, the longitudinal rf field now drives the Rabi

oscillation of the dressed spin qubit. In particular, when $\Delta = 0$, the Rabi frequency of the dressed spin qubit is $\omega_R = \Omega_{2,l}$, where the resonance condition for the rf field is $\omega_2 = \Omega_{1,t}$ [54, 55]. These conditions provide direct experimental access to $\Omega_{2,l}$ and $\Omega_{1,t}$, and could be a very precise approach for characterizing the magnetic field gradient in the system.

With the longitudinal driving, the system can in principle reach the “ultra-strong” driving regime for the dressed qubit, where $\Omega_{2,l} \gg \max(\Delta, \Omega_{1,t}, \omega_2)$. Suppose $\omega_2 > \Omega_{1,t}$, a unitary transformation $U = e^{i\frac{\Omega_{2,l}}{\omega_2}\sigma_Z \sin(\omega_2 t + \phi_2)}$ can be applied, then, the Hamiltonian becomes

$$H'_{driven} \approx \frac{\Delta}{2}\sigma_Z + \sum_n \Omega_{R,n}(\sigma_+ e^{-in(\omega_2 t + \phi_2)} + h.c.), \quad (12)$$

where $\Omega_{R,n} = \Omega_{1,t} J_n\left(\frac{\Omega_{2,l}}{\omega_2}\right)$ and $J_n(x)$ is the Bessel functions of the first kind. When $\Delta \gg \Omega_{1,t}$, the resonance condition becomes $n\omega_2 = \Delta$, and the Rabi frequency is $\omega_R = \Omega_{R,n}$ for the n -th harmonic resonance.

Figure 4 shows the Rabi frequency as a function of the longitudinal gradient $b_{1l} \equiv \partial B_x / \partial x$ when $\Delta = 0$ (black solid line). The red dashed, blue dotted, and brown dash-dotted lines give the Rabi frequencies for $n = 1, 2$, and 3 harmonic resonances when $\Delta = 5 \times 10^6 \text{ s}^{-1}$. When $\Delta = 0$ (resonant microwave driving), the Rabi frequency $\omega_R = \Omega_{2,l}$ shows the normal linear dependence on the driving field amplitude, which is proportional to the longitudinal gradient b_{1l} , with $\Omega_{2,l} \propto b_{1l}$. When $\Delta = 5 \times 10^6 \text{ s}^{-1}$ so that $\omega_2 \approx \Delta/n \gg \Omega_{1,t}$ ($\Omega_{1,t} \sim 5 \times 10^5 \text{ s}^{-1}$ is chosen), higher harmonic resonances become possible, indicating that the system has reached the regime of ultra-strong driving for the dressed spin qubit. In this case, for the $n = 1$ harmonic, the Rabi frequency initially shows a linear b_{1l} dependence, then oscillates (period determined by $\Omega_{2,l}(b_{1l}) \approx \Delta$) as b_{1l} increases. For the $n = 2$ ($n = 3$) harmonic, the Rabi frequency shows a b_{1l}^2 (b_{1l}^3) dependence initially, then oscillates as b_{1l} further increases. Physically, these nonlinear features are a result of the so-called coherent destruction of tunneling, or Landau-Zener-Stückelberg (LZS) interference [56–59]. Among the different multiphoton resonances in Fig. 4, a maximum Rabi frequency of $\omega_R = 10^5 \text{ s}^{-1}$ can be reached. This is faster than the spin dephasing rate, so that such multiphoton resonances are not washed out by dephasing. In addition, the maximum speed of the Rabi oscillation for each multiphoton resonance is achieved at a certain $b_{1,l}$, which also defines optimal field gradients for fast manipulation of a dressed spin qubit.

Here, we emphasize the importance of realizing the ultra-strong longitudinal EDSR. First, one can study the effects of ultra-strong driving on a genuine spin qubit. Secondly, one can

study the LZS interferometry of a single spin, which is an effective tool for characterizing the spin qubit as well as its interaction with the manipulation fields and with the environment [59]. Thirdly, it provides an additional method of spin manipulation especially when dressed state is used for the selective coupling of qubits [60].

Dressed spin qubit proposal— Based on the longitudinal EDSR, we further propose a dressed spin qubit scheme for quantum information processing. The main motivation for the proposal of a dressed qubit is that in certain situations a dressed qubit can help improve system coherence, while maintain sizable two-qubit coupling strength [60]. For example, the sizable $\sigma_X\sigma_X$ coupling is averaged out in the lab frame when the two qubit frequency is off-resonance. The dressed qubit can make use of the $\sigma_X\sigma_X$ coupling for implementation of the fast CZ gate. Moreover, a dressed qubit can be used to achieve selective coupling of two qubits when the frequencies of both qubits are difficult to tune into resonance with a superconducting resonator. Because of the benefit of a dressed qubit, we study further the spin readout, coupling, and decoherence for a dressed qubit.

For the initialization and readout of a dressed qubit, we can make use of the strong longitudinal coupling between a spin qubit and a superconducting resonator. For example, in the dispersive limit ($|\omega_0 - \tilde{\Delta}| \gg g_{s,t}$, where $\tilde{\Delta} = \sqrt{\Delta^2 + \Omega_{1t}^2}$), the state of the dressed qubit can be inferred from the frequency shift of the resonator when the strong coupling limit ($g_{s,t} > 1/T_1, 1/T_2, \kappa$) is achieved, where κ is the decay rate of the superconducting resonator. Moreover, when the transverse driving provides the quantization axis of a dressed qubit, the longitudinal EDSR will provide an extra axis for spin rotation.

One can also couple the spin qubits via the coupling to a superconducting resonator as shown above. In the presence of microwave driving, the effective two-qubit Hamiltonian in the rotating frame is $H_{2Q,DQ} = \sum_i \Delta_i \sigma_{Z,i}/2 + \sum_i \Omega_{1t,i} \sigma_{X,i} + J_{ZZ} \sigma_{Z,i} \sigma_{Z,i}/2 + J_{XX} (\sigma_{+,1} \sigma_{-,2} + \sigma_{-,1} \sigma_{+,2}) + \sum_i \Omega_{2l,i} \sigma_{Z,i} \cos \omega_2 t$. When the frequency of transverse EDSR field on each qubit is near resonance with the microwave driving field ($|\Delta_i| = |\omega_{Z,i} - \omega_1| \ll \Omega_{1t,i}$), the Hamiltonian in the rotating frame is

$$H_{2Q,DQ} = \sum_i \Omega_{1t,i} \sigma_{X,i} + \sum_i \Omega_{2l,i} \sigma_{Z,i} \cos \omega_2 t + \frac{J_{ZZ}}{2} (\sigma_{d+,1} \sigma_{d-,2} + h.c.) + \frac{J_{XX}}{2} \sigma_{X,1} \sigma_{X,2}, \quad (13)$$

where $\sigma_{d\pm,i}$ are the creation and annihilation operators defined for the dressed qubits. Therefore, even when the bare spin splittings $\omega_{Z,i}$ are different for the two qubits, if the near res-

onance condition $|\omega_{Z,i} - \omega_1| \ll \Omega_{1t,i}$ is satisfied, $J_{XX}\sigma_X\sigma_X$ coupling can be realized, which can be used for the CZ gate (spin quantization here is along X -axis due to the strong on-resonance transverse driving). Furthermore, in the absence of longitudinal EDSR, SWAP gate can be realized by J_{ZZ} term. While, in the presence of the longitudinal EDSR and J_{XX} coupling, a resonant CNOT gate for dressed qubits can be realized via selective spin rotation. We emphasize that the above argument is valid for any two qubits among multiple qubits of different qubit splitting that are coupled to a resonator. Therefore, by using a dressed qubit, it is possible to achieve a selective two-qubit gate among multiple qubits, the sizable J_{XX} coupling can be utilized for fast two-qubit gate (without being averaged out to zero if the frequencies of the two qubits are off-resonance), and releases the requirement of tuning the splittings of both qubits into resonance with a resonator, which can be a challenging task in experiments [43].

Finally, we mention briefly the decoherence of a dressed spin qubit. The spin relaxation and dephasing can be modified due to the driving field, where the quantization axis of a dressed qubit is no long along the external magnetic field, but determined by the detuning and driving amplitude. However, the magnitude of relaxation and dephasing of a dressed qubit does not exceeds the relaxation and dephasing of a static spin qubit (see Supplementary information for more details).

III. DISCUSSION

From the above results, it is evident that the spin decoherence, including relaxation and dephasing, can be modified strongly by the symmetry property of the interaction Hamiltonian under time-reversal operation. The B -field dependence of spin relaxation or spin dephasing represents a hallmark to characterize symmetry properties of the SOC Hamiltonian in a system, which may serve as a tool to investigate the possible origin of decoherence in the system. Because of the broken \mathcal{T} -symmetry, there is spin pure dephasing due to $1/f$ charge noise in the presence of longitudinal magnetic field gradient, which suggests the possibility of engineering the magnetic field gradient to effectively minimize the dephasing from the low frequency charge noise. Furthermore, because of the broken \mathcal{T} -symmetry, it becomes possible to achieve the “ultra-strong” electrical driving of a single spin qubit, not observed yet to our knowledge.

We should emphasize that the unified and general understanding of spin relaxation, pure dephasing, and control, and their connection to the \mathcal{T} -symmetry enables us to predict properties in many other physical systems. For example, an electron spin in double or triple QDs with or without a micromagnet. It can also be applied to the case of an electron spin qubit in a hybrid donor-QD [61] or double donor system with different number of nuclei in each donor, where the hyperfine coupling difference provides a longitudinal magnetic field gradient. Furthermore, in a double QD, a position dependent g-factor of an electron spin could arise due to the position dependent SOC (from inhomogeneous electric field) [62, 63], then, the g-factor difference in a double QD also results in an effective SOC that breaks the \mathcal{T} -symmetry. In short, our results can be applied to many different physical systems and may motivate future study on the relation between symmetry and quantum coherence properties in various scenario.

In conclusion, we have studied spin decoherence and control in a QD via a s-SOC generated by a micromagnet. We find that the s-SOC breaks the \mathcal{T} -symmetry, which results in the violation of both the van Vleck cancellation and the longitudinal spin-orbit field cancellation, and thus leads to an effective magnetic field that is different from the case of the i-SOC. In particular, longitudinal effective field is now allowed, while the transverse effective field does not depend on the applied field B_0 . Consequently, the deformation phonon induced spin relaxation shows a B_0^5 dependence, consistent with the recent experiments in a silicon QD at high B_0 field with micromagnets, but in contrast with the B_0^7 dependence normally observed for the i-SOC. In addition, the spin-photon transverse coupling strength shows no dependence with B_0 , compared with the linear B_0 dependence for the case of the i-SOC. Furthermore, the longitudinal effective field gives rise to finite spin pure dephasing from $1/f$ charge noise, contrary to the case of the i-SOC. The longitudinal effective magnetic field also allows possible realization of “ultra-strong” longitudinal EDSR of a spin qubit, which enables additional spin manipulation method and the accurate characterization of the system with a micromagnet. The connection between the effective magnetic field and the \mathcal{T} -symmetry reveals a fundamental property of a spin qubit in a QD. The results could form an important building block for semiconductor spin-based quantum computing.

IV. METHOD

To perform the SW transformation, the explicit form the generator can be obtained. From the model Hamiltonian and the definition of L_d , we have $L_d^{-1}p_x = \frac{im^*}{\hbar}x$ and $L_d^{-1}x = \frac{-i}{\hbar m^* \omega_d^2}(p_x + m^* \omega_c y)$, where $\omega_c = eB_{0z}/(m^*c)$ is the cyclotron frequency. To the lowest order of H_{s-SOC} and E_Z/E_d , the generator S is

$$S \approx L_d^{-1}H_{SOC} = \vec{\sigma} \cdot \vec{\eta}, \quad (14)$$

where $\vec{\eta} = \frac{-ig\mu_B\vec{b}_1}{2\hbar m^* \omega_d^2}(p_x + m^* \omega_c y)$. Then, the noise term becomes $\langle \psi | [S, V_{ext}(\vec{r})] | \psi \rangle = -i\hbar \nabla_p S \cdot \nabla V_{ext} = \frac{1}{2}g\mu_B \vec{\sigma} \cdot \vec{\Omega}$, where the electron is assumed to be in the ground orbital state $|\psi\rangle$.

Details of \mathcal{T} -symmetry of SOC Hamiltonian Here, properties of the SOC under time-reversal are discussed in detail. To be more specific, we denote the Hamiltonian of the synthetic and the intrinsic SOC as H_{s-SOC} and H_{i-SOC} .

For the i-SOC, it can be shown that $L_d^{-1}H_{i-SOC} \propto i\vec{\xi}(x, y) \cdot \vec{\sigma}$, where $\vec{\xi}(x, y)$ is function of position operators [32, 64]. Thus, $L_d^{-1}H_{i-SOC}$ is TRS,

$$T_R L_d^{-1} H_{i-SOC} T_R^{-1} = L_d^{-1} H_{i-SOC}. \quad (15)$$

where T_R is the time-reversal operator (Note $T_R \vec{r} T_R^{-1} = \vec{r}$, $T_R i T_R^{-1} = -i$, and $T_R \vec{\sigma} T_R^{-1} = -\vec{\sigma}$). In contrast, for the s-SOC,

$$T_R L_d^{-1} H_{s-SOC} T_R^{-1} \neq L_d^{-1} H_{s-SOC}, \quad (16)$$

where $L_d^{-1} H_{s-SOC}$ contains TRA term.

Heuristically, these symmetry properties can simply be inferred if we consider an in-plane magnetic field, where the 2D vector potential $\vec{A}(\vec{r})$ vanishes. In this case, \vec{p} is odd under TR: $T_R \vec{p} T_R^{-1} = -\vec{p}$. Given that $H_{i-SOC} \sim p_i \sigma_j$, thus, H_{i-SOC} is TRS. Consequently, $L_d^{-1} H_{i-SOC}$ is also TRS since H_d is TRS; In contrast, since $H_{s-SOC} \sim r_i \sigma_j$, we have H_{s-SOC} and $L_d^{-1} H_{s-SOC}$ to be TRA.

Parameters— For the numeric evaluation, the following values of parameters are used if not specified. We choose $g = 2$, $m^* = 0.19m_0$, and $\hbar\omega_d = 8$ meV for the effective g-factor, the effective mass, and the orbital confinement of an electron in a silicon QD. For the SOC constants, we choose the Rashba constant as $\alpha = 10$ m/s, and the Dresselhaus constant is set to zero for rough estimation. We choose $b_{1t} = b_{1l} = 0.5$ mT/nm for the transverse

and longitudinal field gradient [7]. We choose $v_1 = 5900$ m/s and $v_2 = v_3 = 3750$ m/s for the speed of the different acoustic phonon branches, $\rho_c = 2200$ kg/m³ for the mass density, $\Xi_d = 5.0$ eV and $\Xi_u = 8.77$ eV for the dilation and shear deformation potential constants. The electron temperature is set to be zero for simplicity. We choose the amplitude $A = 1$ μeV for the $1/f$ charge noise, the cutoff frequency $\omega_0 = 1$ s⁻¹, and length scale $l_0 = 100$ nm. In silicon QD, the valley physics can modify spin relaxation at low magnetic field via the spin-valley mixing [34, 65–67]. In this work, we assume that the Zeeman splitting is away from the valley splitting so that the relaxation from spin-valley mixing is suppressed and we will focus on the intra-valley spin-orbit mixing induced spin relaxation and pure dephasing.

For the longitudinal driving of the dressed spin qubit, we choose the following parameters if not specified. We choose the maximum electric field $E_{max} = 10^5$ V/m for both the microwave and the radio-frequency driving, and $\Delta = 5 \times 10^5$ s⁻¹ for the detuning between the microwave and the Larmor frequency of the spin qubit. The transverse field gradient is chosen as 0.01 mT/nm. Note that, to meet the condition of the longitudinal driving more easily in experiments, the maximum electric field can be chosen differently for the microwave and the radio-frequency driving.

V. DATA AVAILABILITY

The data that support the findings of this study are available from the corresponding author upon reasonable request.

VI. CODE AVAILABILITY

The code that support the findings of this study are available from the corresponding author upon reasonable request.

VII. COMPETING INTERESTS

The authors declare no financial or non-financial conflicts of interest.

VIII. AUTHOR CONTRIBUTIONS

P.H. performed derivation and numerical calculation. P.H. and X.H. researched, analyzed, and prepared the manuscript.

IX. FUNDING

P.H. acknowledges supports by the National Natural Science Foundation of China (No. 11904157), the Science, Technology and Innovation Commission of Shenzhen Municipality (No. ZDSYS20170303165926217, No. JCYJ20170412152620376) and Guangdong Innovative and Entrepreneurial Research Team Program (Grant No. 2016ZT06D348); X.H. acknowledges support by US ARO via grant W911NF1710257.

- [1] D. Loss and D. P. DiVincenzo, *Phys. Rev. A* **57**, 120 (1998).
- [2] J. R. Petta, A. C. Johnson, J. M. Taylor, E. A. Laird, A. Yacoby, M. D. Lukin, C. M. Marcus, M. P. Hanson, and A. C. Gossard, *Science* **309**, 2180 (2005).
- [3] R. Hanson, L. P. Kouwenhoven, J. R. Petta, S. Tarucha, and L. M. K. Vandersypen, *Rev. Mod. Phys.* **79**, 1217 (2007).
- [4] J. J. L. Morton, D. R. McCamey, M. A. Eriksson, and S. A. Lyon, *Nature* **479**, 345 (2011).
- [5] F. A. Zwanenburg, A. S. Dzurak, A. Morello, M. Y. Simmons, L. C. L. Hollenberg, G. Klimeck, S. Rogge, S. N. Coppersmith, and M. A. Eriksson, *Rev. Mod. Phys.* **85**, 961 (2013).
- [6] C. Kloeffel and D. Loss, *Annu. Rev. Condens. Matter Phys.* **4**, 51 (2013).
- [7] J. Yoneda, K. Takeda, T. Otsuka, T. Nakajima, M. R. Delbecq, G. Allison, T. Honda, T. Kodera, S. Oda, Y. Hoshi, N. Usami, K. M. Itoh, and S. Tarucha, *Nat. Nanotechnol.* **13**, 102 (2018).
- [8] R. C. C. Leon, C. H. Yang, J. C. C. Hwang, J. C. Lemyre, T. Tanttu, W. Huang, K. W. Chan, K. Y. Tan, F. E. Hudson, K. M. Itoh, A. Morello, A. Laucht, M. Pioro-Ladrière, A. Saraiva, and A. S. Dzurak, *Nat. Commun.* **11**, 1 (2020).
- [9] X. Mi, M. Benito, S. Putz, D. M. Zajac, J. M. Taylor, G. Burkard, and J. R. Petta, *Nature* **555**, 599 (2018).

[10] N. Samkharadze, G. Zheng, N. Kalhor, D. Brousse, A. Sammak, U. C. Mendes, A. Blais, G. Scappucci, and L. M. K. Vandersypen, *Science* **359**, 1123 (2018).

[11] A. J. Landig, J. V. Koski, P. Scarlino, U. C. Mendes, A. Blais, C. Reichl, W. Wegscheider, A. Wallraff, K. Ensslin, and T. Ihn, *Nature* **560**, 179 (2018).

[12] M. Veldhorst, C. H. Yang, J. C. C. Hwang, W. Huang, J. P. Dehollain, J. T. Muhonen, S. Simmons, A. Laucht, F. E. Hudson, K. M. Itoh, A. Morello, and A. S. Dzurak, *Nature* **526**, 410 (2015).

[13] D. M. Zajac, A. J. Sigillito, M. Russ, F. Borjans, J. M. Taylor, G. Burkard, and J. R. Petta, *Science* **359**, 439 (2018).

[14] T. F. Watson, S. G. J. Philips, E. Kawakami, D. R. Ward, P. Scarlino, M. Veldhorst, D. E. Savage, M. G. Lagally, M. Friesen, S. N. Coppersmith, M. A. Eriksson, and L. M. K. Vandersypen, *Nature* (2018), 10.1038/nature25766.

[15] D. M. Zajac, T. M. Hazard, X. Mi, K. Wang, and J. R. Petta, *Appl. Phys. Lett.* **106**, 223507 (2015).

[16] A. R. Mills, D. M. Zajac, M. J. Gullans, F. J. Schupp, T. M. Hazard, and J. R. Petta, arXiv:1809.03976 [cond-mat, physics:quant-ph] (2018), arXiv: 1809.03976.

[17] Y. Tokura, W. G. van der Wiel, T. Obata, and S. Tarucha, *Phys. Rev. Lett.* **96**, 047202 (2006).

[18] M. Pioro-Ladrière, Y. Tokura, T. Obata, T. Kubo, and S. Tarucha, *Appl. Phys. Lett.* **90**, 024105 (2007), publisher: American Institute of PhysicsAIP.

[19] M. Pioro-Ladrière, T. Obata, Y. Tokura, Y.-S. Shin, T. Kubo, K. Yoshida, T. Taniyama, and S. Tarucha, *Nat. Phys.* **4**, 776 (2008).

[20] E. Kawakami, P. Scarlino, D. R. Ward, F. R. Braakman, D. E. Savage, M. G. Lagally, M. Friesen, S. N. Coppersmith, M. A. Eriksson, and L. M. K. Vandersypen, *Nat. Nanotechnol.* **9**, 666 (2014).

[21] X. Wu, D. R. Ward, J. R. Prance, D. Kim, J. K. Gamble, R. T. Mohr, Z. Shi, D. E. Savage, M. G. Lagally, M. Friesen, S. N. Coppersmith, and M. A. Eriksson, *Proc. Natl. Acad. Sci.* **111**, 11938 (2014).

[22] X. Hu, Y.-x. Liu, and F. Nori, *Phys. Rev. B* **86**, 035314 (2012).

[23] M. Benito, J. R. Petta, and G. Burkard, *Phys. Rev. B* **100**, 081412 (2019), publisher: American Physical Society.

[24] F. Borjans, D. M. Zajac, T. M. Hazard, and J. R. Petta, *Phys. Rev. Appl.* **11**, 044063 (2019).

[25] A. Hollmann, T. Struck, V. Langrock, A. Schmidbauer, F. Schauer, T. Leonhardt, K. Sawano, H. Riemann, N. V. Abrosimov, D. Bougeard, and L. R. Schreiber, *Phys. Rev. Appl.* **13**, 034068 (2020), publisher: American Physical Society.

[26] T. Struck, A. Hollmann, F. Schauer, O. Fedorets, A. Schmidbauer, K. Sawano, H. Riemann, N. V. Abrosimov, u. Cywiski, D. Bougeard, and L. R. Schreiber, *NPJ Quantum Inf.* **6**, 1 (2020), number: 1 Publisher: Nature Publishing Group.

[27] R. Li, *Phys. Scr.* **94**, 085808 (2019).

[28] R. Neumann and L. R. Schreiber, *J. Appl. Phys.* **117**, 193903 (2015), publisher: AIP Publishing LLCAIP Publishing.

[29] A. Kha, R. Joynt, and D. Culcer, *Appl. Phys. Lett.* **107**, 172101 (2015).

[30] J. H. Van Vleck, *Phys. Rev.* **57**, 426 (1940).

[31] R. Orbach, *Proc. Natl. Acad. Sci.* **77**, 821 (1961).

[32] V. N. Golovach, A. Khaetskii, and D. Loss, *Phys. Rev. Lett.* **93**, 016601 (2004).

[33] P. Huang and X. Hu, *Phys. Rev. B* **89**, 195302 (2014).

[34] P. Huang and X. Hu, *Phys. Rev. B* **90**, 235315 (2014).

[35] A. V. Khaetskii and Y. V. Nazarov, *Phys. Rev. B* **64**, 125316 (2001).

[36] S. Amasha, K. MacLean, I. P. Radu, D. M. Zumbhl, M. A. Kastner, M. P. Hanson, and A. C. Gossard, *Phys. Rev. Lett.* **100**, 046803 (2008).

[37] R. R. Hayes, A. A. Kiselev, M. G. Borselli, S. S. Bui, E. T. Croke III, P. W. Deelman, B. M. Maune, I. Milosavljevic, J.-S. Moon, R. S. Ross, A. E. Schmitz, M. F. Gyure, and A. T. Hunter, arXiv:0908.0173 [cond-mat] (2009), arXiv: 0908.0173.

[38] M. Xiao, M. G. House, and H. W. Jiang, *Phys. Rev. Lett.* **104**, 096801 (2010).

[39] X. Hu and S. Das Sarma, *Phys. Rev. Lett.* **96**, 100501 (2006).

[40] P. Huang, N. M. Zimmerman, and G. W. Bryant, *NPJ Quantum Inf.* **4**, 62 (2018).

[41] A. Imamoglu, D. D. Awschalom, G. Burkard, D. P. DiVincenzo, D. Loss, M. Sherwin, and A. Small, *Phys. Rev. Lett.* **83**, 4204 (1999).

[42] M. Trif, F. Troiani, D. Stepanenko, and D. Loss, *Phys. Rev. Lett.* **101**, 217201 (2008).

[43] F. Borjans, X. G. Croot, X. Mi, M. J. Gullans, and J. R. Petta, *Nature* **577**, 195 (2020).

[44] A. Blais, R.-S. Huang, A. Wallraff, S. M. Girvin, and R. J. Schoelkopf, *Phys. Rev. A* **69**, 062320 (2004).

[45] C. Kloeffel, M. Trif, P. Stano, and D. Loss, Phys. Rev. B **88**, 241405 (2013).

[46] G. Tosi, F. A. Mohiyaddin, H. Huebl, and A. Morello, AIP Adv. **4**, 087122 (2014).

[47] E. I. Rashba and A. L. Efros, Phys. Rev. Lett. **91**, 126405 (2003).

[48] C. Flindt, A. S. Sørensen, and K. Flensberg, Phys. Rev. Lett. **97**, 240501 (2006).

[49] V. N. Golovach, M. Borhani, and D. Loss, Phys. Rev. B **74**, 165319 (2006).

[50] K. C. Nowack, F. H. L. Koppens, Y. V. Nazarov, and L. M. K. Vandersypen, Science **318**, 1430 (2007).

[51] E. I. Rashba, Phys. Rev. B **78**, 195302 (2008).

[52] J. Stehlik, M. D. Schroer, M. Z. Maialle, M. H. Degani, and J. R. Petta, Phys. Rev. Lett. **112**, 227601 (2014).

[53] J. Stehlik, M. Z. Maialle, M. H. Degani, and J. R. Petta, Phys. Rev. B **94**, 075307 (2016).

[54] A. Laucht, S. Simmons, R. Kalra, G. Tosi, J. P. Dehollain, J. T. Muhonen, S. Freer, F. E. Hudson, K. M. Itoh, D. N. Jamieson, J. C. McCallum, A. S. Dzurak, and A. Morello, Phys. Rev. B **94**, 161302 (2016).

[55] A. Laucht, R. Kalra, S. Simmons, J. P. Dehollain, J. T. Muhonen, F. A. Mohiyaddin, S. Freer, F. E. Hudson, K. M. Itoh, D. N. Jamieson, J. C. McCallum, A. S. Dzurak, and A. Morello, Nat. Nanotechnol. **12**, 61 (2017).

[56] F. Grossmann, T. Dittrich, P. Jung, and P. Hanggi, Phys. Rev. Lett. **67**, 516 (1991).

[57] M. Grifoni and P. Hanggi, Phys. Rep. **304**, 229 (1998).

[58] S. Ashhab, J. R. Johansson, A. M. Zagoskin, and F. Nori, Phys. Rev. A **75**, 063414 (2007).

[59] S. N. Shevchenko, S. Ashhab, and F. Nori, Phys. Rep. **492**, 1 (2010).

[60] J. M. Nichol, L. A. Orona, S. P. Harvey, S. Fallahi, G. C. Gardner, M. J. Manfra, and A. Yacoby, NPJ Quantum Inf. **3**, 3 (2017).

[61] G. Tosi, F. A. Mohiyaddin, V. Schmitt, S. Tenberg, R. Rahman, G. Klimeck, and A. Morello, Nat. Commun. **8**, 450 (2017).

[62] R. M. Jock, N. T. Jacobson, P. Harvey-Collard, A. M. Mounce, V. Srinivasa, D. R. Ward, J. Anderson, R. Manginell, J. R. Wendt, M. Rudolph, T. Pluym, J. K. Gamble, A. D. Baczewski, W. M. Witzel, and M. S. Carroll, Nat. Commun. **9**, 1768 (2018).

[63] T. Tanttu, B. Hensen, K. W. Chan, C. H. Yang, W. W. Huang, M. Fogarty, F. Hudson, K. Itoh, D. Culcer, A. Laucht, A. Morello, and A. Dzurak, Phys. Rev. X **9**, 021028 (2019).

[64] P. Huang and X. Hu, Phys. Rev. B **88**, 075301 (2013).

- [65] C. H. Yang, A. Rossi, R. Ruskov, N. S. Lai, F. A. Mohiyaddin, S. Lee, C. Tahan, G. Klimeck, A. Morello, and A. S. Dzurak, *Nat. Commun.* **4**, 2069 (2013).
- [66] C. Tahan and R. Joynt, *Phys. Rev. B* **89**, 075302 (2014).
- [67] X. Hao, R. Ruskov, M. Xiao, C. Tahan, and H. Jiang, *Nat. Commun.* **5**, 3860 (2014).

X. FIGURE LEGENDS

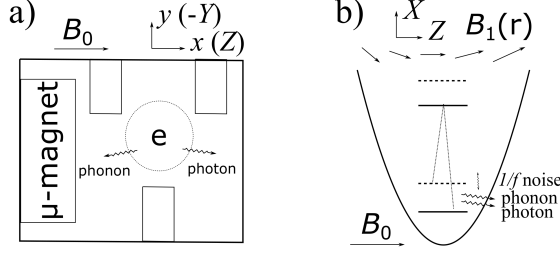


FIG. 1. Schematic diagrams. (a) Schematics of an electron spin qubit in a gate-defined QD next to a micromagnet. (b) Schematics of the electric potential and energy levels in a QD. Inhomogeneous magnetic field \vec{B}_1 from the micromagnet creates a synthetic SOC, which hybridizes the spin-orbit states and leads to the coupling of the spin and electric fields.

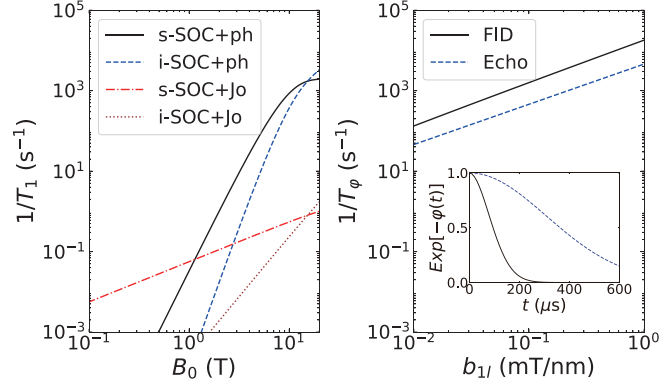


FIG. 2. Spin decoherence. (a) Spin relaxation $1/T_1$ mediated by the s-SOC or the i-SOC as a function of the magnetic field B_0 , where deformation phonon and Johnson noise are considered. (b) Spin pure dephasing $1/T_\varphi$ due to $1/f$ charge noise mediated by the s-SOC as a function of the longitudinal field gradient b_{1l} . Inset of (b): Spin pure dephasing dynamics for free induction decay (FID) or spin echo.

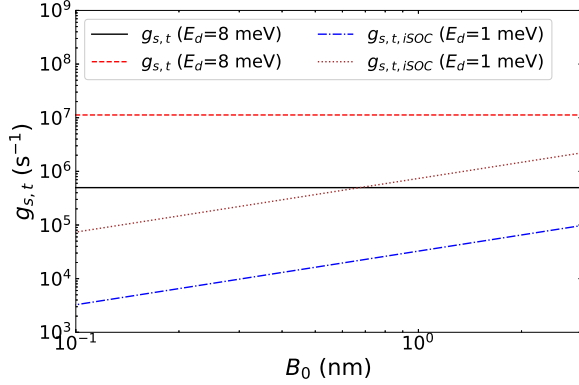


FIG. 3. Transverse spin-photon coupling strength via s-SOC ($g_{s,t}$) or i-SOC ($g_{s,t,iSOC}$) as a function of the magnetic field B_0 .

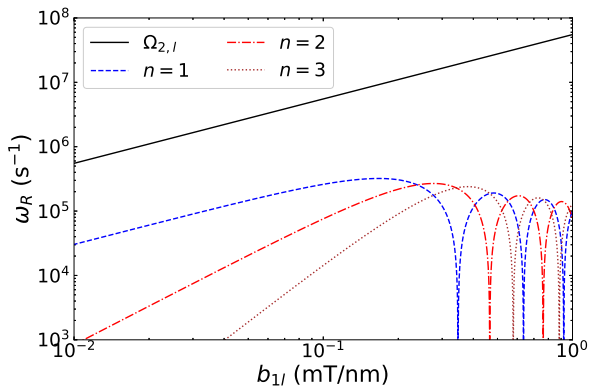


FIG. 4. Rabi frequency of the dressed spin qubit versus the longitudinal field gradient b_{1l} . The solid line is the result when $\Delta = 0$; while the other lines are for the n -th harmonic resonance when $\Delta = 5 \times 10^6 \text{ s}^{-1}$.